MSA UNIVERSITY ENGINEERING JOURNAL

Predicting of Punching Shear Capacity of Corroded Reinforced Concrete Slab-column Joints Using Artificial Intelligence Techniques

Ehab M. Lotfy [1,a], **Ahmed M. Gomaa** [1,2,b], **Sally Hosny**[1,c], **Sherif A. Khafaga**[3,d], **Manar A. Ahmed**[1,e]

1 Department of Civil Engineering, Faculty of Engineering, Suez Canal University, PO Box 41522, Ismailia, Egypt
2 Department of Civil Engineering, The higher institute of engineering and technology Fifth Settlement 11835, Egypt.
3 Building Materials Research and Quality Control Institute, Housing & Building National Research Center (HBRC), Cairo, Egypt
E-mail: [a]Ehablotfy2000@gmail.com, [b]ahmed_blace@eng.suez.edu.eg, [c]Sally_Hosni@eng.suez.edu.eg, [d] sh.khafaga@yahoo.com, [e] manar_abdelshakour@eng.suez.edu.eg.

Abstract

Rebars in reinforced concrete (RC) slab-column structures may corrode under unfavourable conditions, making slab-column joints (SCJs) more susceptible to punching shear (PS) failure. Moreover, PS failure is a common brittle failure, which makes it more difficult to evaluate slab column systems' functioning and failure probability. Thus, the prediction of PS resistance and the related reliability analysis are key factors for building RC slab-column systems. In this study, a high-fidelity finite-element model was created using Abaqus. A comprehensive experimental record is compiled for corroded RC slab-column joints subjected to punching shear loading. Then, effective parameters are established by applying statistical technique principles. The text then provided a model of artificial intelligence, an artificial neural network (ANN). In addition, it provided guidelines

ENGINEERING JOURNAL Volume 2 Issue 2
Received Date January 2023
Accepted Date March 2023
Published Date March 2023
DOI: 10.21608/MSAENG.2023.291880

DOI:10.4186/ej.2009.VOL.ISSUE.pp

for the future development of design codes by identifying the significance of each variable on strength. In addition, it supplied an expression demonstrating the intricate interdependence of affective variables. The results show that The ACI is the most dependable standard, while the CSA is the least. The ANN model had an average, coefficient of variation (COV), root mean square error (RMSE), and lower 95 % values of 0.93, 12.2 %, 1.8, and 0.82, respectively. As a result, the ANN model was found to be more accurate, reliable, and design-safe than variable uncertainty.

Keywords: RC slab-column structure, artificial neural network, Corrosion, Finite element, Punching shear capacity.

1. Introduction

Reinforced concrete (RC) slab-column joint (SCJ) structures consisting of slabs and columns are vulnerable to punching shear (PS) because the beams are not arranged according to structural layout considerations under slabs [1]. Under extreme PS loads, the interior slab-column joint (SCJ) typically collapses first, followed by the other joints, and the overall structure gradually collapses [2], [3]. Numerous experimental studies on the punching shear resistance have been carried out in order to evaluate the behavior of slab-column structures, particularly the slab-column joints (SCJs). According to the experiment results, assessorial models based on different mechanical theories have been developed [4], [5], [14], [6]–[13]. Kinnunen and Nylander [6] analyzed the experimental results of circle slab-circle columns and developed a sector model. Accordingly, Broms [6], [8], [14] developed a modified model taking the effect of size into account, which led to the determination of the slabs' ultimate angle. According to the model for shear stress proposed by Stasio et al.[12], Moe suggested a more effective model that has wider applicability [11], which became the theoretical basis for GB 50010-2010 [10] and ACI 318-19 [7]. After analyzing the critical cracks of SCJs and evaluating the effect of aggregate size, Muttoni suggested the critical shear crack theory (CSCT) [5]. In accordance with the modified compression field theory (MCFT), Wu et al. [4] established a prediction model, and numerous experimental data were used to validate its performance in making predictions. Based on the regression linear analysis results of the experimental data, a prediction model was created by Chetchotisak et al. [13] But, the above mechanical or experimental models have a problem with the accurate prediction [15]–[17]. This study creates a machine learning (ML) analysis based on the Monte Carlo sampling technique (MCS) for reliability analysis to fulfill the needs of real projects. The artificial neural network models are the potential ML models chosen for this article (ANN). Four performance indicators are used to compare the performance of the final prediction models: average, coefficient of variation COV, root mean square error (RMSE), and lower 95 % value. To display the advantages of the ML models, two design provisions (CSA 23.3–14 [18], and ACI 318-19 [7]), as well as two prediction models proposed by Tian et al. [4], and Wu et al. [19], are utilized to compare the prediction performance of ML models. Based on the existing ML model, MCS is used to analyze the dependability of a slab-column structure in a real-world engineering application. In addition, sensitivity analysis is used to debate the assessment of the structure's safety.

2. Methodology

Numerical, theoretical, and machine learning analyses of corroded RC SCJ have been conducted to understand and assess the punching-shear behavior of corroded SCJs. The subsequent work is carried out as follows:

- Finite element analysis has been conducted using Abaqus and verified by Quin et al. experimental program [20], and some variables are studied to get extensive data.
- Comprehensive analysis of available PS strength models for corroded and non-corroded reinforced concrete slabs under PS was collected.

- A model of artificial neural network (ANN) was developed for calculating punching-shear capacity and compared with some design codes.

3. Numerical analysis

3.1. Properties FE modeling of elements and materials

The capacity of SCJs was estimated using the FE model of RC SCJs, and the analysis used was "Dynamic Explicit". The generated numerical FE models in this work use two-node elements T3D2 for the stirrups and three-dimensional (3D) solid elements C3D8R for the concrete and longitudinal reinforcing bars [21]. The brick elements had 50 mm face dimensions after meshing. The Concrete Damaged Plasticity model (CDP) was used because it is more accurate for numeric calculation, and all specification of the damage-plasticity model's parameters has been calculated using Kadhim et al. [22]

3.2. Bond Modeling and Reduction in Concrete and Steel bar Properties

The bond in RC SCJ was simulated using cohesive behavior [21], [23]. Corrosion of steel rebar will lessen the qualities of reinforcement and lead to cracking concrete, which lowers the strength of the concrete. The yield stress, ultimate stress, and elastic modulus of the corroded rebars as well as the concrete compressive strength in the corroded area was corrected to simulate corrosion condition.

3.3. FE model validation

Fig. 1 shows the FE model of the specimen constructed by Qian, et all [20]. All Details of the models which are used for verification are provided in Table 1. Force–displacement diagrams of the numerical models are compared with the results of experimental SCJs, as shown in fig. 2. The PS stress and ultimate displacement of the corroded, and non-corroded SCJs can both be accurately predicted by the FE model, as demonstrated by the fact that each specimen's simulated curve closely resembles its measured curve as shown in fig. 2. The FE simulations' errors are within acceptable bounds, and they closely match the measurements as shown in Table 2.

Table 1. Font type and size list for EJ's template.

Specimen ID	Dimensions (m)	Column size (mm)	d (mm)	fc' (MPa)	Bottom reinforcement (mm)	ρ (%)	Target corrosion degree (%)
S-0	2.2*2.2*0.15	200	118	36.3	T12@105	0.91	0
S-10	2.2*2.2*0.16	200	118	39.3	T12@106	0.91	10
S-20	2.2*2.2*0.17	200	118	41.1	T12@107	0.91	20
S-30	2.2*2.2*0.18	200	118	40.9	T12@108	0.91	30

Table 2. Comparison of ultimate load (kN) and ultimate displacement (mm) between Qian et al experimental program and FEM

specimen ID	Ultimate load, Pu (kN)			Central deflection at Pu (mm)		
	Exp	FE	accuracy	Exp	FE	accuracy
S-0	379.45	367.613	3.12	11.92	12.2381	-2.67
S-10	337.5149905	344.747	-2.14	13.58207899	13.7865	-1.51
S-20	301.9402971	304.244	-0.76	19.74057256	19.011625	3.69
S-30	289.846227	303.88	-4.84	22.13040241	21.86856	1.18

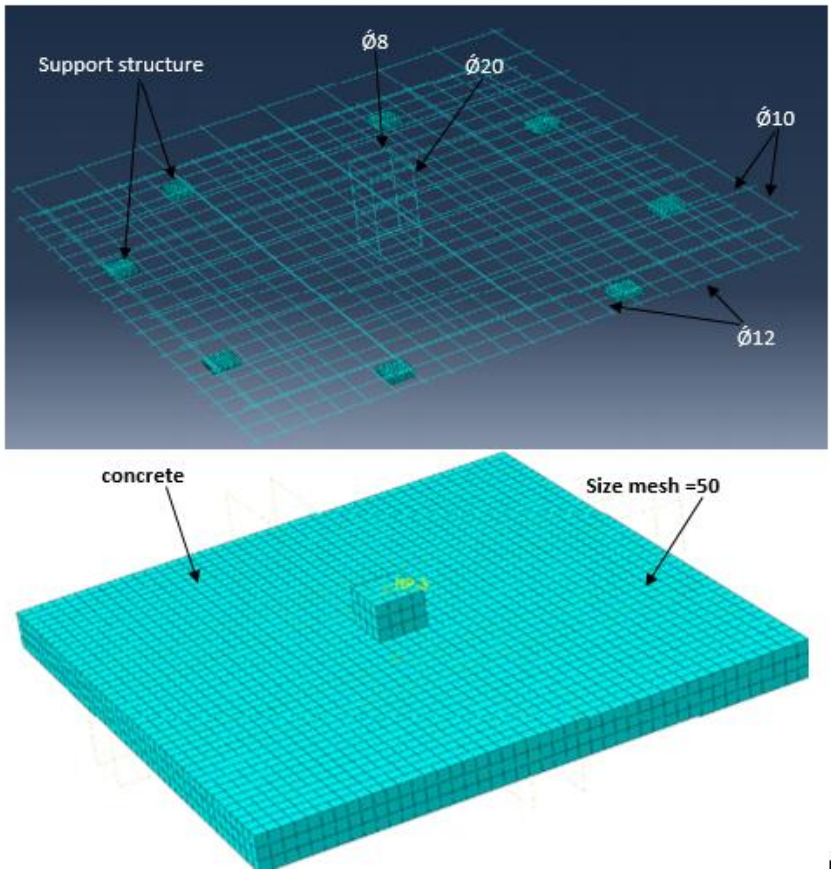

Fig. 1. Finite element model.

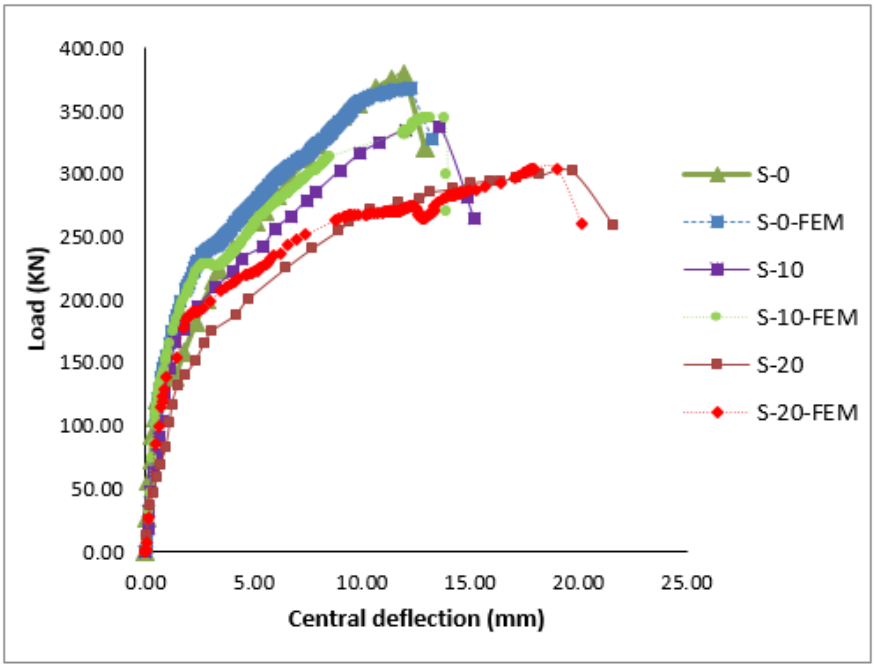

Fig. 2. Test and simulation load-displacement curves are compared.

4. Data Base of Punching Shear Resistance for RC SCJs

The building of ML models requires high-fidelity data; hence the gathering of an experimental database is necessary. The PS resistance database including 119 results is displayed in Table 3 (Appendix. A), and the statistical data of input factors are presented in Table 4. Several papers indicate that SCJs are influenced by eight primary factors: column's cross-sectional area (X1), effective depth of a slab (X2), compressive strength of concrete (X3), span depth ratio (X4), reinforcement ratio (X5), column rectangularity (X6), yield strength of reinforcement (X7), and corrosion degree (X8). Their distributions are classified by minimum, maximum, standard deviation, and average as shown in Table 4. The aim of the ML models is to predict the PS resistance (Y) of SCJs. The relative frequency distributions of the input factors are depicted by the histograms in Fig. 3 [24]–[26].

Table 4. Descriptive statistics of variables

Input factors	Notation	Min	Average	Std. Dev	Max
The cross-section area of column (mm2)	X1	3025	28256.933	20558.38	160000
Slab's effective depth (mm)	X2	29.7	104.80756	35.65166	170
Compressive strength of concrete (MPa)	X3	18.2	33.710756	6.384261	45.6
Span depth ratio	X4	6.3	11.2	3.6461	20.0
Reinforcement ratio (%)	X5	0.2	1.0528571	0.429116	2.3
Column rectangularity	X6	1	1.3319328	0.754302	4
Yield strength of reinforcement (MPa)	X7	280	456.66555	87.76229	744
Corrosion degree (%)	X8	0	5.8907563	8.52294	30
Punching shear capacity (kN)	Y	30.5	205.96696	103.9359	480

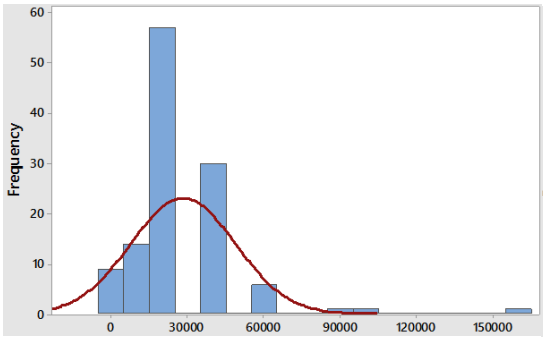

(X1) cross-section area of column

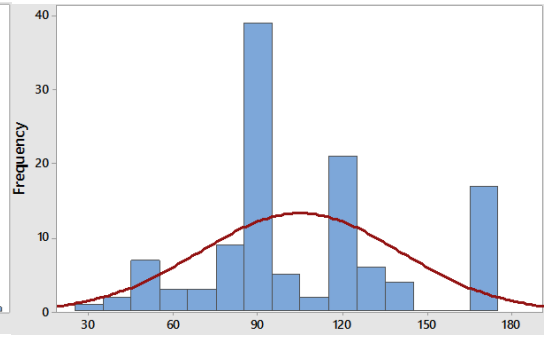

(X2) slab's effective depth

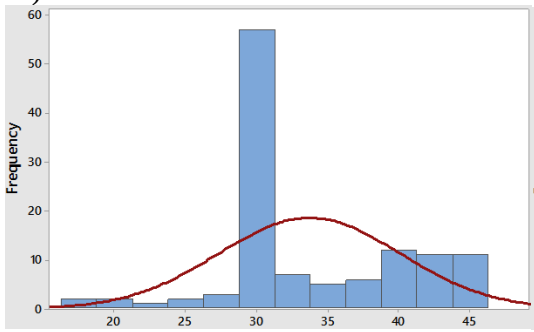

(X3) compressive strength of concrete

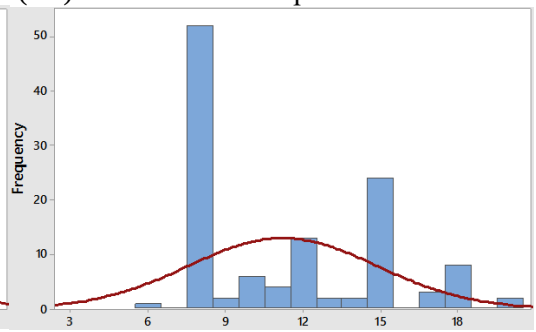

(X4) span depth ratio

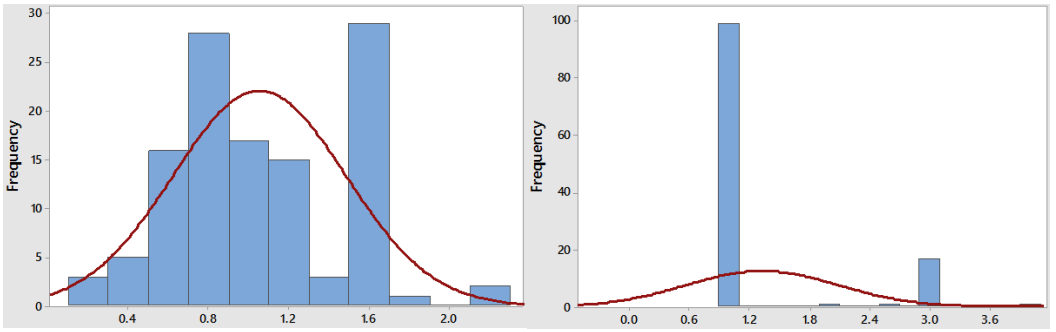

(X5) reinforcement ratio (X6) column rectangularity

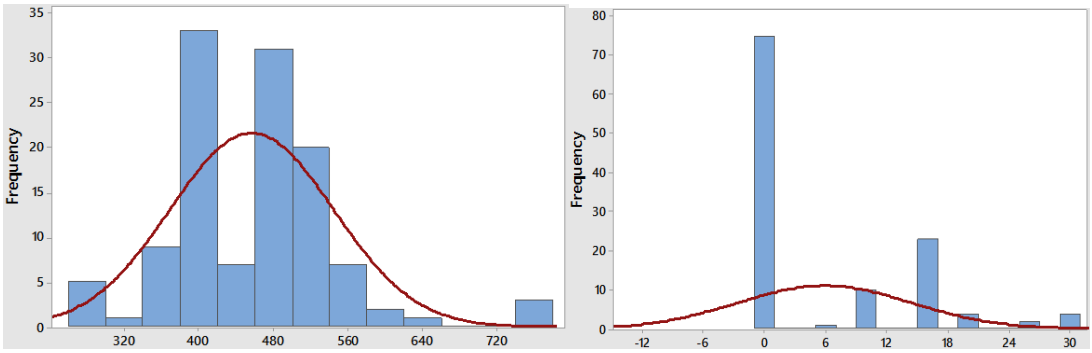

(X7) yield strength of reinforcement (X3) corrosion degree

Fig. 3. Histograms of input variables.

5. Construction of Machine Learning (ML) models

5.1. Introduction

The application of machine learning (ML) to predict the PS capacity of corroded reinforced concrete (RC) SCJs has been discussed seldom, with just a handful of research accessible in the published literature. The artificial neural network (ANN) is made up of several processing components known as neurons. Neurons are interconnected via linkages known as weights. Initially, during training, weights are set arbitrarily; they are then adjusted by comparing the predicted values to the actual values, and the mistakes are backpropagated through the network to minimize the observed errors. The construction of a three-layer ANN is illustrated in fig. 4. It consists of K number of inputs, L number of neurons in the hidden layer, and M number of outputs, demonstrating the potential of ANN to predict multiple outputs simultaneously and emphasizing the strength of ANN. The ANN training procedure consists of three primary steps: (1) Initialization of internal parameters; (2) Evaluation of the model; and (3) Updating the internal variables to obtain the best points. The network weights are updated using backpropagation, which is a mechanism for fine-tuning the weights of an ANN depending on the error rate achieved in the previous training cycle. The primary benefit of ANN is its capacity to capture complicated correlations between input and output variables without previous knowledge of the nature of these interactions. However, adopting the

conventional gradient descent approach for ANN training might result in significant inaccuracies and local minima [27]. Consequently, the first ANN model suggested is trained using gradient descent with two key alterations. The suggested model is trained using 119 records of available experimental data, as shown in Table 5.

Table 5. Training Summary for ANN

Parameter	**Description**
Neurons in the input layer	8
Neurons in the output layer	1
The hidden layer activation function	Sigmoid
Output layer activation function	Linear
Cost function	MSE
Number of hidden layers	1
Number of training iterations	10

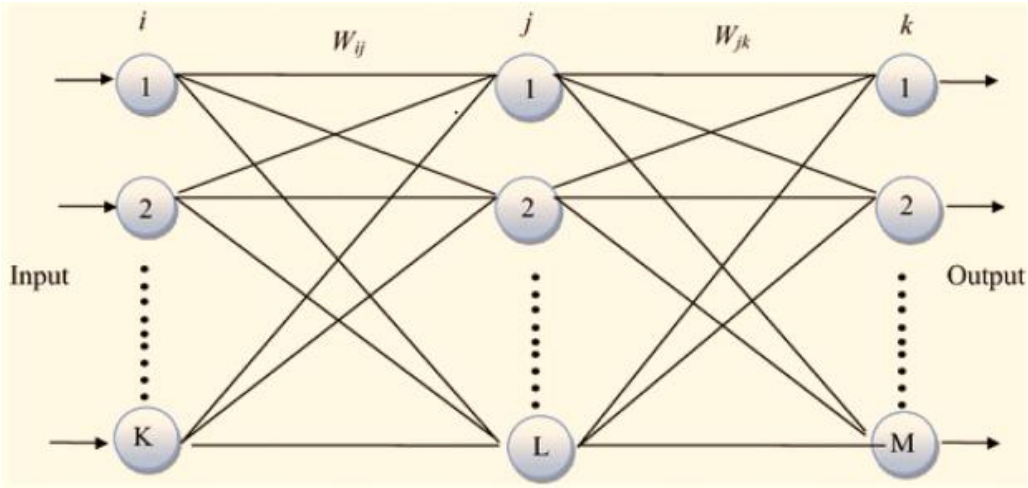

Fig. 4. Three-layer ANN Structure.

5.2. The ANN models

There are four primary training approaches for ANNs: Gradient Descent (ANN-GD), Quasi-Newton method (ANN-QN), Levenberg-Marquardt (ANN-LM), and Conjugate Gradient (ANN-CG). Choosing the best training approach is difficult since certain training

techniques may work for one type of problem but not another [27]. Comparing traditional ANN- GD to other approaches, it exhibits promising, trustworthy outcomes [28] wherein the errors between the actual experimental results and the expected results from the trained model are reduced [29] and can easily adapt to the complex behavior of the training data. The goal of ANN- GD, often regarded as the most well-liked optimization strategy in machine learning, is to locate the coefficients that reduce the error function to the greatest extent feasible by locating a local minimum of a differentiable function. It calculates the change in all weights in relation to the change in error [30], [31]. The conventional ANN-GD is a training model that updates its weights and biases in the direction of the performance function's negative gradient, as follows:

$$w^{(i+1)} = w^{(i)} - \nabla f\ (w^{(i)})\ \eta^{(i)} \quad \text{Eq.1}$$

where $w^{(i)}$ are the weights in the ith iteration , $\nabla f\ (w^{(i)})$ is the gradient of the loss function f in $w^{(i)}$, and $\eta^{(i)}$ is the rate of learning ith iteration. In the training process, the learning rate η is a hyperparameter that regulates the changes to the model, i.e., How quickly the model adapts to the given problem, relative to the evaluated error in each training iteration, maybe the most important hyperparameter when configuring the network, where too high values for η may result in a model that converges too quickly to a suboptimal model and a too small value may result in an unstable model, as depicted in fig. 5. The challenge is in determining the correct η value.[32]. ANN-GD is utilized with several changes, such as an adjustable learning rate and the addition of a momentum term, to improve performance and training stability. This model employs an adjustable learning rate, with a default value of 0.01, which is typical for standard ANN-GD. Afterward, it is changed based on performance measurements throughout training. If at the conclusion of each training iteration, the performance declines in the direction of our aim, then the learning rate is raised by the factor η_{inc} = 1.05. If performance grows by more than a certain factor during the training phase, it is reduced by a factor of η_{dec} = 0.7. Training is quicker and more consistent when an adjustable learning rate is used. Gradient descent with momentum and backpropagation of the adaptive learning rate is the training approach employed. The momentum term (m_c) aids in accelerating convergence without reducing the model's capacity to solve nonlinear issues. Backpropagation is used to update the network weights; it is a method for fine-tuning the weights of an ANN depending on the error rate achieved during the previous training iteration. it is derived using the performance (p) derivatives with respect to the weight and bias variables × For each training iteration i. Each variable is modified based on gradient descent with momentum.

$$d_{x(i)} = mc * d_{x(i-1)} + \frac{\eta * mc * d_p}{d_x} \quad \text{Eq.2}$$

where $d_{x(i-1)}$is the previous change in the weights or bias, mc is the momentum coefficient, x is the weights and bias, and (d_p) is the derivative of the performance. The used training approach is capable of training any network whose weight, inputs and transfer functions contain derivative functions. The ANN model learns from the experimental database of corroded RC slabs to determine the PS capacity. As shown in fig. 6, the model comprises an input layer, a hidden layer with 15 neurons, and an output layer. The model is

trained using the following inputs: cross-section area of column (X1), slab's effective depth (X2), compressive strength of concrete (X3), span depth ratio (X4), reinforcement ratio (X5), column rectangularity (X6), yield strength of reinforcement (X7), and corrosion degree (X8). the output is the prediction of the PS capacity of corroded RC SCJ. Our trained model will terminate training if any of the following conditions are met: a) the maximum number of training iterations is reached, b) the maximum amount of time has elapsed, or c) the performance target has been reached. The stopping criterion in our model was the third condition. The model was trained with 119 records from a dataset. According to recommendations for optimal performance evaluation, the dataset is separated into two major sections [33]: the training set comprised 70 % of the entire data, while the remaining 30 % was used for testing and validation. The dataset was utilized without any additional processing. fig. 7 demonstrates that the model converges at the 10-training iteration, but the best performance was achieved at the 4-training iteration. The error numbers for the training, validation, and testing phases are depicted in fig. 8. Additionally, a linear fit is given to each case and plotted. Fig. 9 depicts a regression model that displays the ANN model's correlation between real and predicted values. Pearson Correlation Coefficient R =0.91, 0.94, and 0.91 for training, validation, and testing, respectively.

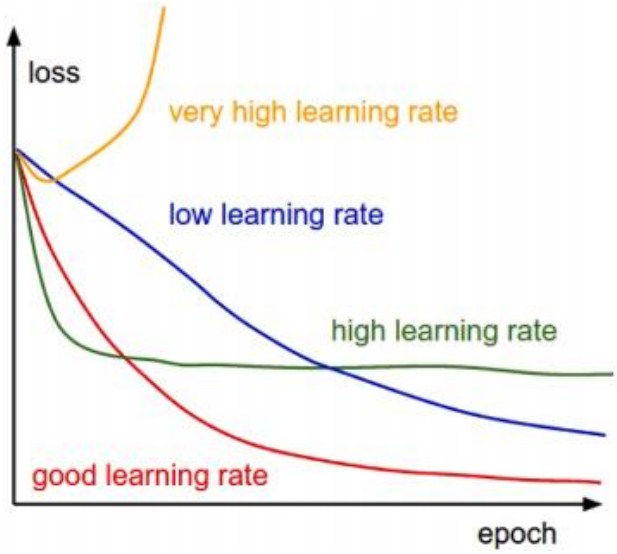

Fig. 5. The effect of learning rate on the training process[33].

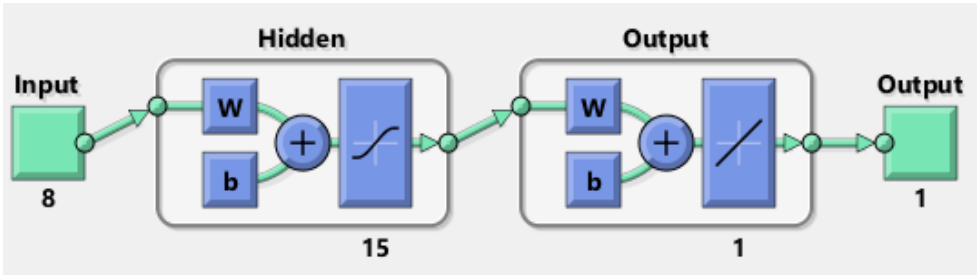

Fig. 6. ANN- GD training model.

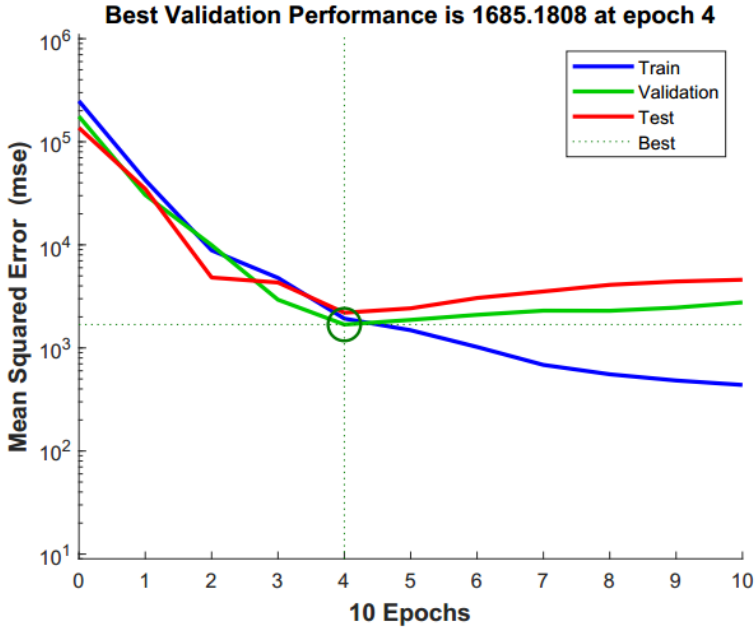

Fig. 7. The performance of the ANN-GD training process.

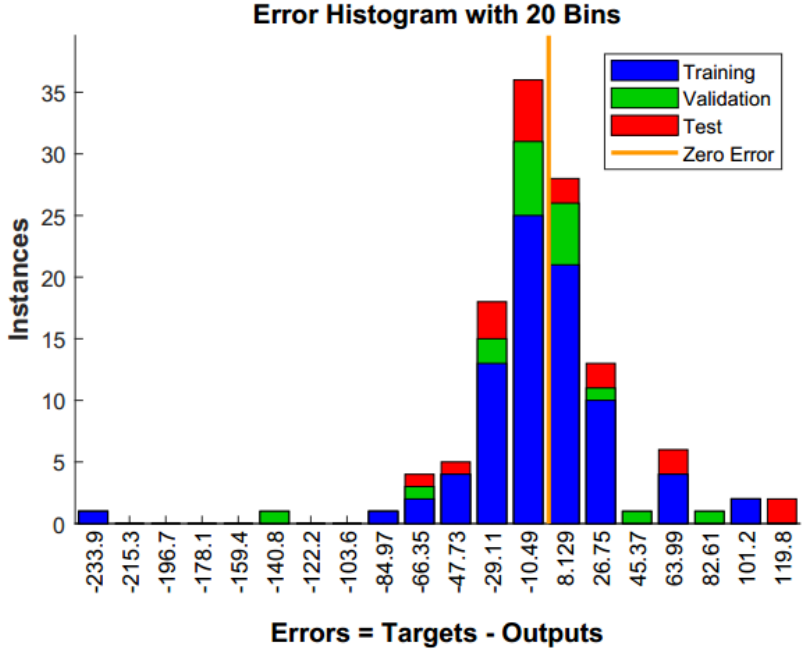

Fig. 8. The errors of ANN-GD

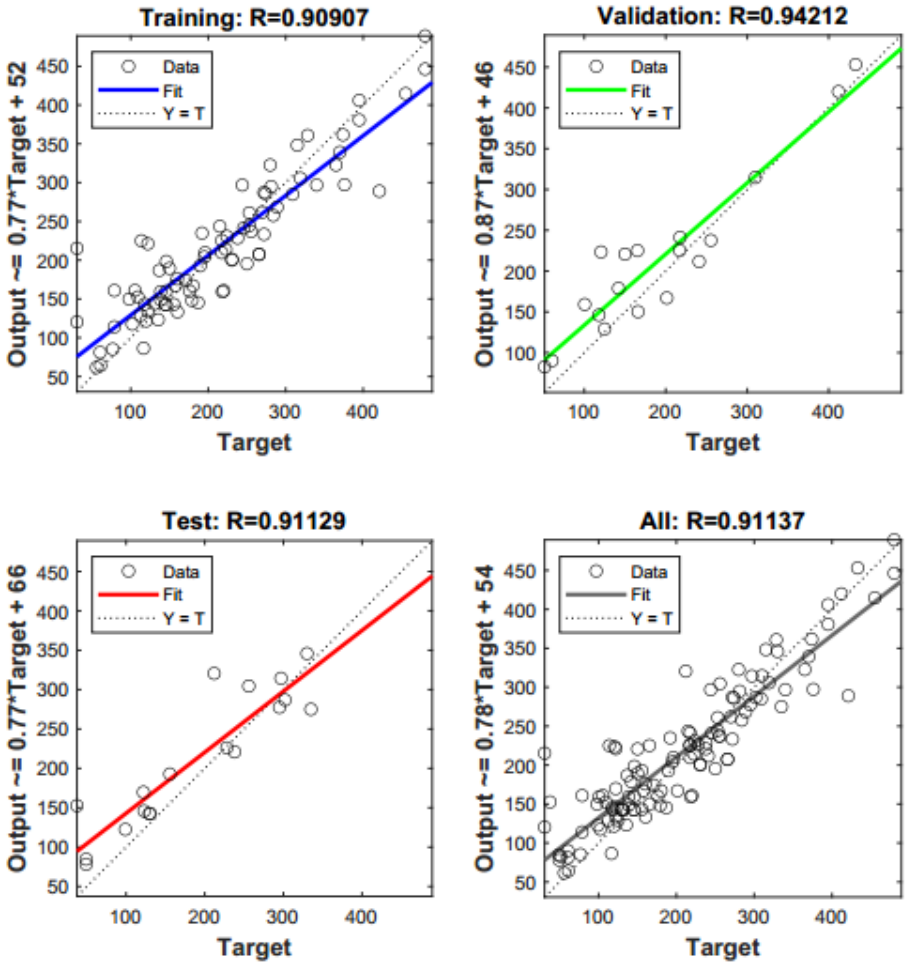

Fig. 9. Regression Analysis for ANN-GD model training, validation, and testing.

6. Comparison between proposed models and selected models

To assess the efficacy of the proposed models, four statistical measures were computed for the proposed model and the chosen models: Average, coefficient of variation COV, root mean square error RMSE, and lower 95 % value. fig. 10 depicts a comparison of the selected and proposed models. Based on these four statistical measures, the proposed models are reliable, consistent, and reasonably safe for design. Whereas the ANN model's average coefficient of variation, root mean square error, and lower 95 % value, respectively, were 0.93, 12.2%, 1.8, and 0.82.

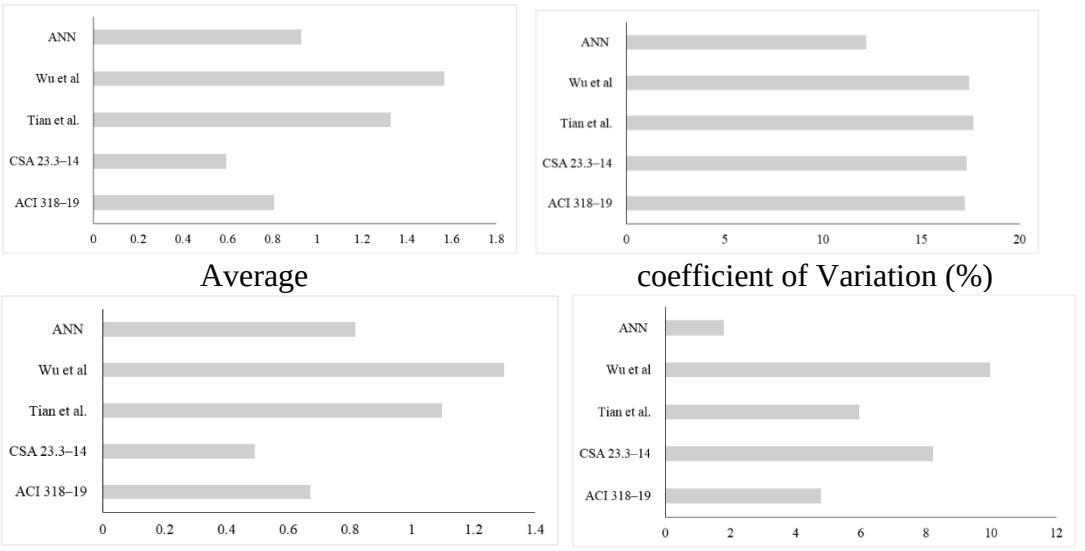

Fig. 10. Comparison between all models.

7. Conclusion

This study examined the punching-shear behavior of corroded RC slab-column joints. According to the numerical, theoretical, and machine learning analysis of corroded RC SCJ, the following conclusions can be drawn:

- The FE simulations' errors are within acceptable bounds, and they closely match the measurements.
- The PS capacity and displacement of the uncorroded and corroded SCJ specimens can both be accurately predicted by the FE model.
- Based on the average, coefficient of variation (COV), root mean square error (RMSE), and lower 95 % value the selected models were found to need further investigation.
- It is noted that The ACI is the most reliable among the selected models and the CSA the least reliable.
- The ANN model was found to be more accurate, consistent, and reasonably safe for design compared to variable uncertainty.

Appendix A

Table. 3 Experimental databases for corroded RC SCJs under punching shear

X1	X2	X3	X4	X5	X6	X7	X8	Y	paper
40000	118	36.3	14.7	0.91	1	532	0	376	(Qian et al., 2022)
40000	118	39.3	14.7	0.91	1	435	10	335	(Qian et al., 2022)
40000	118	41.1	14.7	0.91	1	412	20	302	(Qian et al., 2022)
40000	118	40.9	14.7	0.91	1	399	30	289	(Qian et al., 2022)
40000	118	43.7	14.7	0.52	1	532	0	280	(Qian et al., 2022)
40000	118	44.1	14.7	0.52	1	471	10	244	(Qian et al., 2022)
40000	118	45.6	14.7	0.52	1	448	20	212	(Qian et al., 2022)
40000	118	40.5	14.7	0.52	1	396	30	192	(Qian et al., 2022)
40000	93	37.6	17.6	1.16	1	532	0	274	(Qian et al., 2022)
40000	93	41.1	17.6	1.16	1	423	10	238	(Qian et al., 2022)
40000	93	41.3	17.6	1.16	1	401	20	228	(Qian et al., 2022)
40000	93	41.5	17.6	1.16	1	380	30	215	(Qian et al., 2022)
40000	93	43.7	14.7	0.52	1	532	0	270	(Qian et al., 2022)
40000	93	44.1	14.7	0.52	1	471	10	250	(Qian et al., 2022)
40000	118	43.7	14.7	0.52	1	532	0	365	(Qian et al., 2022)
40000	118	44.1	14.7	0.52	1	471	10	340	(Qian et al., 2022)
40000	143	43.7	14.7	0.52	1	532	0	480	(Qian et al., 2022)
40000	143	44.1	14.7	0.52	1	471	10	455	(Qian et al., 2022)
40000	118	43.7	14.7	0.74	1	532	0	330	(Qian et al., 2022)
40000	118	44.1	14.7	0.74	1	471	10	310	(Qian et al., 2022)

40000	118	43.7	14.7	1.18	1	532	0	412	(Qian et al., 2022)
40000	118	44.1	14.7	1.18	1	471	10	395	(Qian et al., 2022)
40000	118	43.7	14.7	1.52	1	532	0	480	(Qian et al., 2022)
40000	118	44.1	14.7	1.52	1	471	10	433	(Qian et al., 2022)
62500	104	40	18.3	1	1	532	0	370	(Mahmoud et al., 2016)
62500	104	40	18.3	1	1	471	26	297	(Mahmoud et al., 2016)
62500	138	21	14.5	2.2	1	530	0	374	(Kim & Lee, 2021)
10000	80	20.18	12.5	0.34	1	530	0	109.34	(Yooprasertchai et al., 2021)
10000	55	31.9	11.5	0.34	1	533	0	49.2	(Harajli & Soudki, 2003)
10000	55	35.5	11.5	0.73	1	545	0	60.5	(Harajli & Soudki, 2003)
10000	75	35.5	8.4	0.34	1	540	0	78.8	(Harajli & Soudki, 2003)
10000	75	29.1	8.4	0.73	1	565	0	122	(Harajli & Soudki, 2003)
22500	70	25.8	17.4	1	1	530	0	160.3	(El Maaddawy & Soudki, 2003)
62500	120	33	16.6	0.97	1	520	0	30.5	(Taresh et al., 2021b)
4000	120	28.9	16.6	1	1	740	0	272	(Filatov & Galyautdinov, 2018)
100000	120	22.3	18.3	1	2.5	744	0	281.3	(Filatov & Galyautdinov, 2018)
160000	120	25.6	20.0	1	4	740	0	328.4	(Filatov & Galyautdinov, 2018)
6400	85	30	10.0	0.43	1	510	0	160.033	(Jaafer et al., 2019)
22500	120	35	8.5	0.97	1	385	0	222.68	(H. Abdel-Kareem, 2020)
22500	90	30	11.0	0.97	1	385	0	150	(Shaaban et al., 2013)
3600	45	30	11.6	0.2	1	280	0	55.76	(Ye et al., 2021)
3600	45	30	11.6	0.6	1	280	0	76.7	(Ye et al., 2021)
3600	45	30	11.6	1.4	1	280	0	99.01	(Ye et al., 2021)

3600	45	30	11.6	2.3	1	280	0	112.5	(Ye et al., 2021)
3600	45	30	8.3	1.4	1	280	0	116.5	(Ye et al., 2021)
62500	130	33	14.3	1.07	1	385	0	309	(Taresh et al., 2021b)
16900	102	36.5	12.0	0.46	1	601	0	224	(Madkour et al., 2021)
40000	90	44	15.0	1	1	455	0	253	(Madkour et al., 2021)
14400	40	32	18.3	0.25	1	556	0	37.5	(Madkour et al., 2021)
10000	80	44.4	12.0	0.71	1	510	0	157.5	(Madkour et al., 2021)
62500	105	27.1	8.4	0.59	1	492	0	284	(Madkour et al., 2021)
10000	80	40	12.0	0.85	1	570	0	166	(Madkour et al., 2021)
16900	102	36.8	12.0	1.4	1	601	0	295	(Madkour et al., 2021)
16900	97	40.4	12.0	0.8	1	625	0	272	(Madkour et al., 2021)
22500	92	42.4	11.4	1.84	1	420	0	241	(Madkour et al., 2021)
40000	129	39	14.7	0.56	1	520	0	256	(Madkour et al., 2021)
40000	129	39	14.7	0.87	1	520	0	315	(Madkour et al., 2021)
40000	129	39	14.7	1.18	1	520	0	395	(Madkour et al., 2021)
22500	110	44	12.0	1.2	1	455	0	253	(Bertagnoli et al., 2019)
90000	140	30	20.0	0.7	1	570	0	319	(Mohamed & Khattab, 2020)
40000	90	33	8.0	1.26	1	570	0	122	(Neamah & Al-Ramahee, 2021)
22500	80	18.2	10.0	1.2	1	385	0	113.7	(C. C. Chen & Chen, 2020)
22500	80	27.6	10.0	1.2	1	385	0	136.8	(C. C. Chen & Chen, 2020)
22500	80	18.2	10.0	0.6	1	385	0	145.9	(C. C. Chen & Chen, 2020)
22500	80	27.6	10.0	0.6	1	385	0	176.1	(C. C. Chen & Chen, 2020)
10000	45	31.9	12.1	0.59	1	487.6	0	49.2	(Harajli & Soudki, 2003)

10000	45	35.5	12.1	0.83	1	487.6	0	60.5	(Harajli & Soudki, 2003)
10000	65	35.5	8.9	0.74	1	488.5	0	78.8	(Harajli & Soudki, 2003)
10000	65	29.1	8.9	1.04	1	488.5	0	122	(Harajli & Soudki, 2003)
40000	130	29	13.3	1	1	410	0	421	(Sharaf et al., 2006)
10000	90	29	12.0	0.23	1	375	0	30.5	(Silva et al., 2021a)
3025	29.7	43.2	10.0	1.2	1	400	0	51.31	(Alhussainawe et al., 2017)
3025	39.7	38.6	8.3	1.2	1	400	0	61.02	(Alhussainawe et al., 2017)
3025	59.7	38.6	6.3	1.2	1	400	0	135.53	(Alhussainawe et al., 2017)
22500	90	30	7.8	1.57	3	380	15	138.617	FEM
22500	170	30	7.8	0.89	3	385	15	130.65	FEM
22500	90	30	7.8	1.57	1	385	15	129.4497	FEM
22500	170	30	7.8	1.57	1	485	0	245.65	FEM
22500	90	30	7.8	1.57	3	485	0	217.519	FEM
22500	170	30	7.8	0.89	3	380	15	155.63	FEM
22500	90	30	7.8	1.57	3	485	0	196	FEM
22500	170	30	7.8	1.57	1	485	0	217.519	FEM
22500	90	30	7.8	1.57	3	368	15	178.98	FEM
22500	90	30	7.8	0.89	1	485	0	265.65	FEM
22500	90	30	7.8	0.89	3	365	15	138.617	FEM
22500	90	30	7.8	0.89	3	485	0	255.36	FEM
22500	170	30	7.8	1.57	3	365	15	105.36	FEM
22500	170	30	7.8	1.57	1	365	15	120.6	FEM
22500	90	30	7.8	1.57	1	386	15	145.36	FEM

22500	170	30	7.8	0.89	1	485	0	230.65	FEM
22500	90	30	7.8	1.57	1	485	0	217.519	FEM
22500	170	30	7.8	1.57	3	485	0	218.365	FEM
22500	170	30	7.8	1.57	1	380	15	237.89	FEM
22500	170	30	7.8	0.89	1	380	15	189.65	FEM
22500	170	30	7.8	0.89	1	380	15	155.63	FEM
22500	90	30	7.8	0.89	3	380	15	220	FEM
22500	90	30	7.8	0.89	1	380	15	187	FEM
22500	90	30	7.8	0.89	1	480	0	265.65	FEM
22500	170	30	7.8	1.57	3	480	0	145.6	FEM
22500	170	30	7.8	0.89	3	480	0	180.365	FEM
22500	90	30	7.8	1.57	1	480	0	165.325	FEM
22500	170	30	7.8	0.89	3	480	0	201.36	FEM
22500	170	30	7.8	0.89	1	480	0	230.65	FEM
22500	90	30	7.8	0.89	1	370	15	130.65	FEM
22500	170	30	7.8	1.57	3	377	15	100.56	FEM
22500	90	30	7.8	0.89	3	468	0	255.36	FEM
22500	90	30	7.8	1.57	1	485	0	217	FEM
22500	90	31.3	7.8	1.57	1	480	5	195	FEM
22500	90	31.1	7.8	1.57	1	447	10	171	FEM
22500	90	30.3	7.8	1.57	1	385	15	145	FEM
22500	90	30.3	7.8	1.57	1	377	20	125	FEM
22500	90	30.3	7.8	1.57	1	360	25	120	FEM

22500	90	30.3	7.8	1.57	1	334	30	102	FEM
22500	90	30.3	7.8	1.57	2	385	15	118	FEM
22500	90	30.3	7.8	1.57	3	385	15	98	FEM
22500	130	30.3	7.8	1.57	1	385	15	142	FEM
22500	170	30.3	7.8	1.57	1	385	15	150	FEM
22500	90	30.3	7.8	0.89	1	385	15	118	FEM
22500	90	30.3	7.8	1.12	1	385	15	123	FEM

8. References

[1] A. Yazarlu and M. Dehestani, "Application of discrete element method (DEM) in characterization of bond-slip behavior in RC beams with confinement subjected to corrosion," Structures, vol. 28, no. August, pp. 1965–1976, 2020, doi: 10.1016/j.istruc.2020.10.026.

[2] H. R. Taresh, M. Y. M. Yatim, and M. R. Azmi, "Punching shear behaviour of interior slab-column connections strengthened by steel angle plates," Eng. Struct., vol. 238, no. November 2020, p. 112246, 2021, doi: 10.1016/j.engstruct.2021.112246.

[3] A. H. Abdel-Kareem, "Punching Strengthening of Concrete Slab-column Connections Using Near Surface Mounted (NSM) Carbon Fiber Reinforced Polymer (CFRP) Bars," J. Eng. Res. Reports, vol. 9, no. 2, pp. 1–14, 2020, doi: 10.9734/jerr/2019/v9i217013.

[4] L. Wu, T. Huang, Y. Tong, and S. %J B. Liang, "A Modified Compression Field Theory Based Analytical Model of RC Slab-Column Joint without Punching Shear Reinforcement," vol. 12, no. 2, p. 226, 2022.

[5] A. Muttoni, "Punching shear strength of reinforced concrete slabs without transverse reinforcement," ACI Struct. J., vol. 105, no. 4, pp. 440–450, 2008, doi: 10.14359/19858.

[6] S. Kinnunen and H. Nylander, Punching of concrete slabs without shear reinforcement. Elander New York, 1960.

[7] M. I. American Concrete Institute ACI Committee %J American Concrete Institute ACI Committee: Farmington Hills USA, "Building Code Requirements for Structural Concrete ACI 318-19 and Commentary 318R–19," 2019.

[8] C. E. %J A. C. I. S. J. Broms, "Elimination of flat plate punching failure mode," vol. 97, no. 1, pp. 94–101, 2000.

[9] A. H. Rahman, Effect of steel corrosion on the strength of slab-column connections. National Research Council Canada, Institute for Research in Construction, 1992.

[10] L. Shen, Y. Shen, and S. Liang, “Reliability Analysis of RC Slab-Column Joints under Punching Shear Load Using a Machine Learning-Based Surrogate Model,” Buildings, vol. 12, no. 10, 2022, doi: 10.3390/buildings12101750.

[11] C.-C. Chen and S.-L. %J A. S. Chen, “Strengthening of reinforced concrete slab-column connections with carbon fiber reinforced polymer laminates,” vol. 10, no. 1, p. 265, 2019.

[12] J. Di Stasio, “Transfer of bending moment between flat plate floor and column,” in Journal Proceedings, 1960, vol. 57, no. 9, pp. 299–314.

[13] P. Chetchotisak, P. Ruengpim, D. Chetchotsak, and S. Yindeesuk, “Punching Shear Strengths of RC Slab-Column Connections: Prediction and Reliability,” KSCE J. Civ. Eng., vol. 22, no. 8, pp. 3066–3076, 2018, doi: 10.1007/s12205-017-0456-6.

[14] C. E. Broms, “Concrete flat slabs and footings: Design method for punching and detailing for ductility,” KTH, 2005.

[15] H. D. Nguyen, G. T. Truong, and M. %J E. S. Shin, “Development of extreme gradient boosting model for prediction of punching shear resistance of r/c interior slabs,” vol. 235, p. 112067, 2021.

[16] S. Mangalathu, H. Shin, E. Choi, and J.-S. %J J. of B. E. Jeon, “Explainable machine learning models for punching shear strength estimation of flat slabs without transverse reinforcement,” vol. 39, p. 102300, 2021.

[17] A. A. Manar and T. M. Mansour, “Modelling of Shear Strength for Reinforced Concrete Beams Provided with Side-Face Reinforcement in Dependence of Crack Inclination Angle,” vol. 4, no. 6, 2019.

[18] P. Adebar, J. G. Mutrie, R. DeVall, and D. Mitchell, “Seismic design of concrete buildings: The 2015 Canadian building code,” NCEE 2014 - 10th U.S. Natl. Conf. Earthq. Eng. Front. Earthq. Eng., 2014, doi: 10.4231/D39W09032.

[19] Y. Shen, L. Wu, and S. %J E. F. A. Liang, “Explainable machine learning-based model for failure mode identification of RC flat slabs without transverse reinforcement,” vol. 141, p. 106647, 2022.

[20] K. Qian, J. S. Li, T. Huang, Y. H. Weng, and X. F. Deng, “Punching shear strength of corroded reinforced concrete slab-column connections,” J. Build. Eng., vol. 45, no. August 2021, p. 103489, 2022, doi: 10.1016/j.jobe.2021.103489.

[21] H. A. Al-Sakkaf, “Modelling of corroded reinforced concrete beams,” no. May, pp. 1–94, 2016.

[22] M. M. A. Kadhim, A. Jawdhari, A. H. Adheem, and A. Fam, “Analysis and design of two-way slabs strengthened in flexure with FRCM,” Eng. Struct., vol. 256, no. October 2021, 2022, doi: 10.1016/j.engstruct.2022.113983.

[23] M. A. Shayanfar, A. Hatami, M. Zabihi-Samani, B. Babakhani, and A. R. Faroughi, “Simulation of the force-displacement behavior of reinforced concrete beams under di erent degrees and locations of corrosion,” Sci. Iran., vol. 29, no. 3A, pp. 964–972, 2022, doi: 10.24200/SCI.2021.55422.4214.

[24]Y. Tian, “Behavior and Modeling of Reinforced Concrete Slab-Column Connections,” p. 210, 2007.

[25] M. Zhang, M. Deng, Z. Wu, and J. Pan, “Flexural cracking behavior and calculation approach of reinforced highly ductile fiber-reinforced concrete beams,” Arch. Civ. Mech. Eng., vol. 21, no. 4, pp. 1–14, 2021, doi: 10.1007/s43452-021-00309-0.

[26] M. A. L. Silva, J. C. P. H. Gamage, and S. Fawzia, “Performance of slab-column connections of flat slabs strengthened with carbon fiber reinforced polymers,” Case Stud. Constr. Mater., vol. 11, p. e00275, 2019, doi: 10.1016/j.cscm.2019.e00275.

[27] M. A. L. Silva, K. V Dedigamuwa, and J. C. P. H. Gamage, “Performance of severely damaged reinforced concrete fl at slab-column connections strengthened with Carbon Fiber Reinforced Polymer,” Compos. Struct., vol. 255, no. April 2020, p. 112963, 2021, doi: 10.1016/j.compstruct.2020.112963.

[28] T. Nguyen, H. Ly, H. T. Mai, and V. Q. Tran, “On the Training Algorithms for Artificial Neural Network in Predicting the Shear Strength of Deep Beams,” vol. 2021, 2021.

[29] M. T. K. Niazi, J. Ahmad, F. Alqahtani, F. A. B. Baotham, and F. %J E. Abu-Amara, “Prediction of critical flashover voltage of high voltage insulators leveraging bootstrap neural network,” vol. 9, no. 10, p. 1620, 2020.

[30] M. Ganzha and L. Maciaszek, Communication Papers of the 2020 Federated Conference on Computer Science and Information Systems, vol. 23. 2020.

[31] S. Sharma, S. Ahmed, M. Naseem, W. S. Alnumay, S. Singh, and G. H. Cho, “Pre-Parametric Project Cost and Soil Shear-Strength Estimation in Construction and Geotechnical Engineering,” 2021.

[32] H. De Vries, R. Memisevic, and A. Courville, “Deep Learning Vector Quantization,” no. April, pp. 27–29, 2016.

[33] I. Mansouri, T. Ozbakkaloglu, O. Kisi, and T. Xie, “Predicting behavior of FRP-confined concrete using neuro fuzzy, neural network, multivariate adaptive regression splines and M5 model tree techniques,” Mater. Struct. Constr., vol. 49, no. 10, pp. 4319–4334, 2016, doi: 10.1617/s11527-015-0790-4.